Azimuthal motion, reorientation, cessation, and reversal of the large-scale circulation in turbulent thermal convection: A comparative study in aspect ratio one and one-half geometries

Heng-Dong Xi and Ke-Qing Xia
Department of Physics, The Chinese University of Hong Kong, Shatin, Hong Kong, China
(Received 5 May 2008; published 30 September 2008)

We report a systematic experimental study of the orientation and the flow strength of the large-scale circulation (LSC) in water-filled cylindrical Rayleigh-Bénard convection cells with aspect ratios 2.3, 1, and 0.5 by both direct velocity measurement and the indirect multithermal-probe measurement. Unlike its weak effect in the system's global heat transport, the aspect ratio Γ is found to play an important role in the dynamics of the azimuthal motion of the LSC. It is found that in larger Γ geometries the azimuthal motion of the LSC's vertical plane is confined in smaller azimuthal region than that in smaller Γ geometries. The twisting motion between top and bottom parts of the LSC observed in the $\Gamma=1$ geometry is found to be absent in the $\Gamma=1/2$ case. It is found that in the $\Gamma=1/2$ geometry the orientational change $|\Delta\phi|$ through a reorientation has an exponential distribution, in contrast to the power-law distribution for the $\Gamma=1$ case. Despite the difference in orientational change, the occurrence of the reorientations is a Poisson process in both geometries. Using the conditional average of the time interval between adjacent cessations or reversals on the rebound flow strength, we demonstrate the possibility to empirically predict when the next cessation or reversal will most likely occur if the rebound flow strength of the preceding cessation or reversal is given.

DOI: 10.1103/PhysRevE.78.036326 PACS number(s): 47.27.−i, 05.65.+b, 47.55.P−, 91.25.Mf

I. INTRODUCTION

Rayleigh-Bénard (RB) convection is a fluid layer heated from below and cooled from the top. The fluid is set to motion when the applied temperature difference exceeds a critical value. The dynamics of the flow is determined by the geometry of the cell and two dimensionless parameters: the Rayleigh number $\mathrm{Ra}=\alpha g\Delta T H^3/(\nu\kappa)$ and the Prandtl number $\mathrm{Pr}=\nu/\kappa$, where ΔT is the applied temperature difference, H is the height of the cell, g is the acceleration due to gravity, and α, ν, and κ are, respectively, the volume expansion coefficient, kinematic viscosity, and thermal diffusivity of the fluid. The lateral confinement of the convective flow due to the existence of the sidewall is characterized by the aspect ratio $\Gamma=D/H$, where D is the diameter of the cylindrical cell used. RB convection receives extensive studies not only because it is a model system for the study of buoyancy-driven fluid turbulence but also because of its importance in the understanding of the ubiquitous convection phenomenon occurring in nature, for example, those in astrophysical and geophysical systems such as solar and mantle convections [1,2].

At sufficiently high value of Ra, a large-scale circulation, in the form of a single roll comparable to the size of the convection cell, emerges [3–5] (see Fig. 1). The various aspects of this large-scale circulation (LSC) have been studied extensively over the years, using experimental, numerical, and theoretical approaches [6–18]. Through these studies, it is now generally believed that, in $\Gamma=1$ cells, the laterally separated warm and cold plumes rise and fall along the two opposing sidewall regions, thus driving the bulk fluid in the cell interior [8,10,11,19,20]. For the $\Gamma=1/2$ geometry, direct velocity measurements showed that the time-averaged large-scale flow is also of a single-roll structure [8,12]. A numerical study suggests that the flow structure in this geometry can be either single-roll or double-roll, depending on the Ra, Pr, and the sidewall used [16]. In a recent experimental study, we found that both the single-roll and double-roll structures exist in $\Gamma=1$, $1/2$, and $1/3$ geometries. Our systematic study of flow mode transitions further showed that in $\Gamma=1$ and $1/2$ geometries, the large-scale convective flow is overall a single-roll structure, while in the $\Gamma=1/3$ geometry the flow spends only one-third of time in the single-roll flow mode [21].

Figure 1 is a shadowgraph image showing the spatial structure of LSC in a $\Gamma=1$ cell, which is captured simulta-

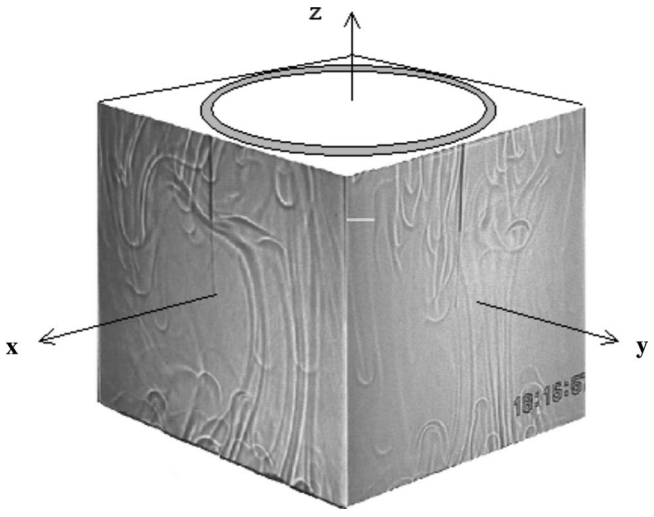

FIG. 1. Instantaneous shadowgraph images of the convective flow in an aspect ration unity cylindrical cell taken simultaneously from two vertical planes at 90° angle. The convecting fluid is Dipropylene glycol at $\mathrm{Pr}=1032$, $\mathrm{Ra}=8.3\times10^8$. A rectangular jacket is glued to the outside of the cylindrical cell to reduce optical distortions due to the curvature of the cell.

neously by two CCD cameras separated by 90° in a horizontal plane. When viewed from the positive x direction the fluid rises on the right and sinks on the left, suggesting that the flow is overall a single-roll structure. When viewed from the positive y direction the fluid goes up vertically within a narrow band near the central region of the cell. Combining the two views together we can conclude that the flow in the convection cell is a quasi-two-dimensional (2D) single-roll structure with a finite width of about half cell diameter. The self-organized process of formation and sustenance of this single-roll structure from individual plumes has been elucidated convincingly in a recent experiment using both flow visualization and quantitative velocity measurements [20]. Since the LSC is a quasi-2D structure, it may rotate azimuthally. The LSC's vertical circulating plane has indeed been found to undergo constant azimuthal meandering in both mercury [7,22] and water [12,23–25] convections. For the $\Gamma=1$ geometry, in addition to the overall azimuthal meandering, the upper half and the lower half of the LSC are also found to undergo a twisting oscillation with a 180° phase difference [26]. Occasionally the LSC will experience larger reorientations which can be accomplished by two scenarios. One is by rotation of the LSC's circulating plane during which the flow strength shows no appreciable variation, this is called rotation-led reorientation; the other involves a temporary vanishing of the flow strength—a cessation of the LSC [23], with the LSC restarting at a new orientation, which is called a cessation-led reorientation. Note that a cessation does not necessarily produce a reorientation, because after a cessation the LSC could restart from the same azimuthal position where it stops. If the cessation is accomplished by an orientational change of 180°, it is a flow direction reversal of the LSC. Reversals have been observed in two-dimensional numerical simulations of RB convection [27] and is the subject of a number of recent model studies [28–32]. In addition to its importance in understanding the dynamics of turbulent flows in the RB system [28,33] and in other turbulent systems [34], the putative connection of this phenomenon to similar reversals in the magnetic polarity of the Earth [35] and in the wind direction in the Earth's atmosphere [36] also makes it of more general interest. Ahlers and co-workers [23,25] showed that the reorientation of the LSC plane is the major dynamic event compared to the much rarer reversals. Specifically, they found that, in $\Gamma=1$ geometries, the orientational change after reorientation $|\Delta\phi|$ is power law distributed, i.e., no special $|\Delta\phi|$ exists and reorientation with small orientational change is more probable. They further showed that after a cessation, the orientational change $|\Delta\phi|$ is uniformly distributed, i.e., the LSC can restart at any new orientation with equal probability after a cessation.

Compared to the extensive studies in $\Gamma=1$ geometry, there are relatively few experimental studies focused on the azimuthal motion of the LSC in $\Gamma=1/2$ geometry. Recently Sun, Xi, and Xia found that in $\Gamma=1/2$ cells the meandering of the LSC orientation is diffusive over short time scales, and in longer time scales it generates a net rotation [12]. These properties, which were first observed in $\Gamma=1/2$ cells [12], were later confirmed in $\Gamma=1$ cells [24,25]. Sun, Xi, and Xia also suggested that the origin of the observed net rotation is the Earth's Coriolis force [12]. The effect of the Earth's Coriolis force to the azimuthal motion of the LSC was later systematically studied in detail for $\Gamma=1$ geometry [37]. In a recent study Xi and Xia showed that in $\Gamma=1/2$ geometry cessations not only can occur, they do so with much higher probability than those in the $\Gamma=1$ case with about one third of the cessations being reversal events [38]. With this large number of reversal events, detailed statistical analysis of unambiguously identified cessation-led reversals became possible. For example, it is found that the time interval between successive reversals is exponentially distributed, suggesting that the occurrence of the reversals is a Poisson process [38]. Since the dynamics of cessations and reversals are very different in $\Gamma=1$ and $1/2$ geometries, it is natural to ask whether other dynamical events such as the azimuthal motion and the reorientation of the LSC are the same in these two geometries.

In this paper, we report an experimental study of the azimuthal motion of the LSC in cylindrical convection cells of different aspect ratios, using water as the working fluid. Direct velocity measurements are made in cells with aspect ratios $\Gamma=2.3$, $\Gamma=1$, and $\Gamma=1/2$, respectively, and we find that the aspect ratio plays an important role in the dynamics of the LSC. We then make a comparative study of the properties of reorientation in $\Gamma=1$ and $1/2$ geometries. Long time measurements of both the orientation and the flow strength of the LSC are made simultaneously. Detailed analysis reveals that the dynamics of reorientation of the LSC in the two geometries appear to be governed by different mechanisms.

The remainder of this paper is organized as follows. In Sec. II we describe the convection cells and experimental methods. We then discuss the properties of the azimuthal motion of the LSC in different geometries in Sec. III. Section III A shows the overall features of the LSC's azimuthal motion in different aspect ratio geometries, where results from direct velocity measurement ($\Gamma=2.3$, 1, and $1/2$) and from the multithermal-probe measurement over much longer period of time ($\Gamma=1$ and $1/2$) are presented. The oscillatory and diffusive motions of the LSC's azimuthal orientation are discussed in Sec. III B. In Sec. III C we show that the LSC has different properties for reorientation events in $\Gamma=1$ and $1/2$ cells. In Sec. III D, we show how the time interval between adjacent events of cessations or reversals is related to the rebound strength of the LSC after such an event. We conclude and summarize our findings in Sec. IV.

II. APPARATUS AND EXPERIMENTAL METHODS

A. The convection cell

Two types of cells are used in the experiment and water is the convecting fluid in both cases. The details of the cells used in the PIV velocity measurement and in the multithermal-probe measurement have been described in Refs. [24,39], respectively. We give only their essential features here. The first type, used in the PIV measurement, referred to as the sapphire cell, consists of a 5-mm-thick sapphire disc as top plate and a 1.4-cm-thick copper disc as bottom plate. The use of the sapphire plate is to make the top plate optically accessible. Plexiglas cylindrical tubes of inner

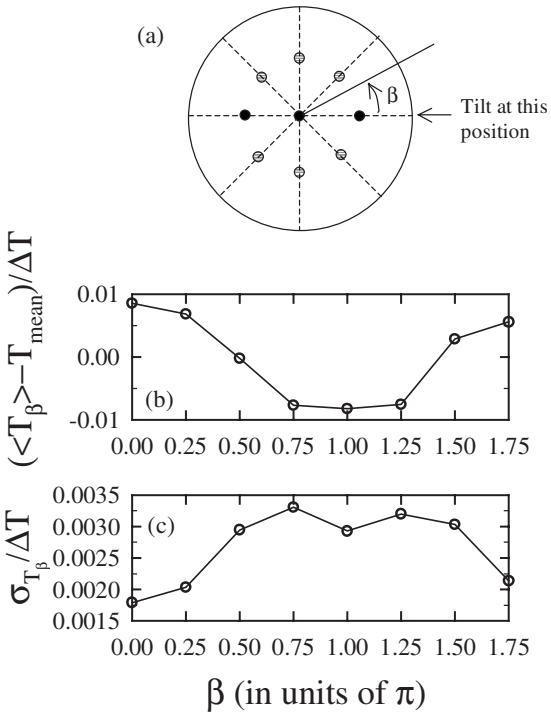

FIG. 2. The sketch (top view) of the bottom plate and the arrangement of the thermistors (the circles) embedded in the plate (a). The azimuthal profile of the normalized mean temperature (b) and r.m.s. temperature (c) measured by the thermistors embedded in the bottom plate. Here T_{mean} is the mean temperature of the plate and ΔT is the temperature difference across the top and bottom plates.

diameter 18.5 cm and wall thickness 8 mm are used as the sidewalls. The separations between the top and bottom plates are 8.0, 18.5, and 37.0 cm so that the aspect ratios of the cells are respectively, $\Gamma=2.3$, 1, and $1/2$. The second type of cell, used in the multithermal-probe measurement, referred to as copper cell, has 1-cm-thick copper discs as its top and bottom plates and a Plexiglas tube of inner diameter 19 cm and wall thickness 5 mm as the sidewall. Two plexiglas tubes with height 19.0 and 38.0 cm are used, thus resulting in the aspect ratio $\Gamma=1$ and $1/2$, respectively.

During the experiments, for both the sapphire cell and the copper cell, constant power is supplied to the bottom plate of the convection cell, so that it is under a constant-flux boundary condition, but at steady state its temperature remains effectively constant; the top plate's temperature is regulated by a refrigerated circulator (Polyscience, 9702), so that it is under constant-temperature boundary condition. Since the constant temperature boundary condition of the bottom plate is achieved by constant heat flux, to examine the temperature inhomogeneity of bottom plates, we made an independent measurement using the same apparatus. The measurements are in the $\Gamma=1$ copper cell for $\mathrm{Ra}=5.0\times10^9$, $\Delta T=31$ °C. In this measurement we have three thermistors embedded in the bottom plate along a diameter, one at the center and the other two at half-radius positions, which are represented by the three solid circles in Fig. 2(a). To lock the azimuthal orientation of the LSC, we tilted the convection cell with 2° at azimuthal angle $\beta=0$. The temperatures at the angular positions 0 and π and plate center were first measured, these positions are denoted by the the solid circles. To achieve azimuthal resolution of $\pi/4$ of the temperature measurements in the plates, we repeat the measurement after the cell is rotated by $\pi/4$, $\pi/2$, and $3\pi/4$ with respect to the tilt position, so that temperatures in angular positions $\pi/4$, $\pi/2$, $3\pi/4$, $5\pi/4$, $3\pi/2$, and $7\pi/4$, which are denoted by the open circles, are effectively measured with respect to the LSC orientation. Each measurement lasts for 48 h, which is about 5000 times of the LSC turnover time for that Ra, and therefore is statistically sufficient. In this way, we have obtained mean temperatures of bottom plates in radial and azimuthal directions. These data reveal that the temperature at positions where hot plumes are emitted from plate is higher than that at the positions where the cold plumes arrive the plate, as shown in Fig. 2(b). The mean temperature at plate center is almost the same as the mean temperature of the plate T_{mean}. Although the spatial temperature difference is small—the hottest position is only about 0.5 °C hotter than the coldest position (only 1.7% of ΔT), it is a manifestation of the existence of the LSC, and could be used to identify the orientation and flow strength of the LSC [7,22]. The calculated r.m.s. temperatures of bottom plate in azimuthal directions [Fig. 2(c)] show that all the r.m.s. temperature less than 0.35% of ΔT. The r.m.s. temperature of plate center, which is not shown in the figure, is about 0.21% of ΔT. The measured r.m.s. values also show that the temperature fluctuations are larger at where the plumes arrive at the plate than those from where plumes are emitted, which is consistent with a recent measurement made in the 1-m diameter Hong Kong Big Cell [40]. We have shown the temperature distribution of the bottom plate for the tilted case. For the leveled cell case, the LSC will explore larger azimuthal range [41], thus both the spatial and temporal variations will be slightly smaller. Based on the small spatial and temporal variations of the plate temperatures we conclude that our experiments are approximately under the constant temperature boundary condition.

B. Experimental methods

Two methods are used to measure the orientation and the flow strength of the LSC. One is direct PIV velocity measurement, the other is multithermal-probe method. The direct velocity measurement is carried out in the sapphire cell. The PIV system and the selection criteria for the operating parameters in turbulent thermal convection have been given in Refs. [9,11], and the measurement of the two-dimensional (2D) horizontal velocity field in a $\Gamma=1$ cell has also been described in detail in Ref. [24]. Here we just give a brief introduction to the method, a laser lightsheet of thickness ~2 mm is shone horizontally through the sidewall of the cell at a distance of 1 cm below the top sapphire plate, where the horizontal velocity is maximum as found by previous velocity measurements made in the LSC's vertical plane [11,12]. The measuring area covers the entire horizontal cross section of the cell and contains 709 velocity vectors. As in Ref. [24], we define a velocity $\vec{V}_{LSC}$ to represent the overall direction and magnitude of the velocity field in the horizontal plane $\vec{V}_{LSC}(t)=V_x(t)\hat{i}+V_y(t)\hat{j}$, where V_x and V_y are respective spa-

tial averages of the local velocities $v_x(t)$ and $v_y(t)$ over the measuring area. From $\vec{V}_{\mathrm{LSC}}$ the speed or magnitude of the LSC $V_{\mathrm{LSC}} \equiv |\vec{V}_{\mathrm{LSC}}| = (V_x^2 + V_y^2)^{1/2}$ and its azimuthal orientation $\theta = \arctan(V_y/V_x)$ are obtained. Here θ is defined within $[0°, 360°]$, this definition leads to artificial and sudden changes when the orientation of LSC plane changes from 360° to 0° or vice versa. To eliminate the artificial jumps we use another quantity ϕ, $\phi = \theta \pm 2n \times 360°$, to extend the range of azimuthal angle from $[0°, 360°]$ to $[-\infty, +\infty]$. Anticlockwise direction is defined as positive when viewed from the top.

As the PIV method is not practical for long-time measurement, we use the multithermal-probe method to obtain better statistics. This method takes advantage of the fact that the LSC is essentially an organized flow of thermal plumes [20] and that when it flows up (down) along the sidewall it carries hot (cold) fluid. Therefore by measuring the relative temperature differences along the perimeter of the sidewall [23,25,38] (or along the plates [7]), the orientation and strength of the LSC can be obtained. This method has been used in $\Gamma = 1$ cells by Ahlers and co-workers [23,25], was extended to $\Gamma = 1/2$ and $1/3$ cases by Xi and Xia [21,38]. Here we give only a brief description of this method. Twenty-four blind holes were drilled from the outside into the sidewall in such a way that they distribute in three horizontal rows at heights $H/4$, $H/2$, and $3H/4$ from the bottom and in eight vertical columns equally spaced azimuthally around the cylinder. The end of these holes has a distance of 0.7 mm from the fluid-contact surface. Twenty-four thermistors were placed into the blind holes until they touched the end snugly. The thermistors were connected to a multichannel multimeter and their resistances were measured at a sampling frequency of 0.29 Hz, which were then converted into temperatures using measured calibration curves. By fitting the function $T_i = T_0 + A\cos(i\pi/4 - \theta)$, $i = 0, \ldots, 7$, separately at each time step, to the eight temperatures in one row, we obtain amplitude A, which is a measure of the strength of the flow at that height, and θ, which gives the azimuthal orientation of the flow (the angular position at which the hot fluid comes up) at the corresponding height [23]. We then similarly convert θ to the continuous variable ϕ. Again, anticlockwise direction is defined as positive when viewed from the top. The typical errors of the fitting are 16% for A and 13° for θ.

Experiments using the PIV technique are made in the sapphire cell at the fixed Prandtl number Pr=5.3, and are conducted only at one or a few values of Ra for each Γ. For the systematic multithermal-probe measurement, which were conducted in the copper cells, the Ra is varied from 9.0×10^8 to 6.0×10^9 for $\Gamma = 1$ geometry and from 1.6×10^{10} to 7.2×10^{10} for $\Gamma = 1/2$ geometry. To achieve better statistics, two extra-long measurements lasting 31 days and 34 days are conducted in the $\Gamma = 1$ and $1/2$ copper cells, at $\mathrm{Ra} = 5.6 \times 10^9$ and $\mathrm{Ra} = 5.7 \times 10^{10}$, respectively, using the multithermal-probe method. It is found that the measurements by the two methods give the same results for all the statistical properties. Because results from the 24 thermistors provide a more complete picture on the overall state of flow in the system, unless stated otherwise all results presented below come from the multithermistor measurements.

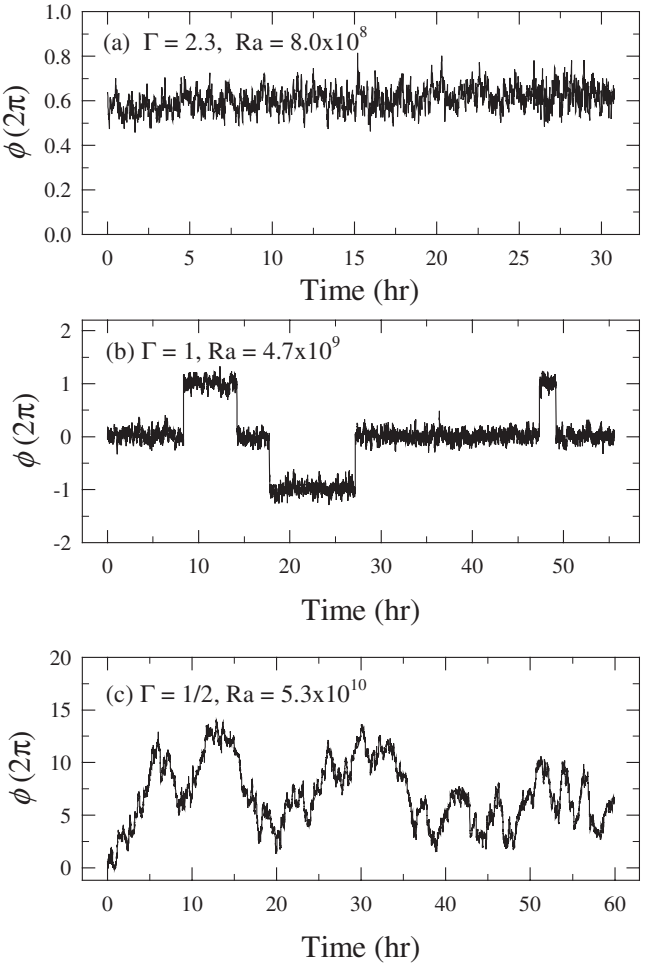

FIG. 3. The time series of the orientations of LSC obtained by direct velocity measurement for (a) $\Gamma = 2.3$ ($\mathrm{Ra} = 8.0 \times 10^8$), (b) $\Gamma = 1$ ($\mathrm{Ra} = 4.7 \times 10^9$), (c) $\Gamma = 1/2$ ($\mathrm{Ra} = 5.3 \times 10^{10}$). Note: the $\Gamma = 1$ data is reproduced here from Fig. 4 of Ref. [24] for comparison.

In the PIV measurements, the convection cells are leveled to within $0 \pm 0.2°$. After an improvement in the levelling method (see the Appendix for details), the convection cells are leveled to within $0 \pm 0.057°$, which is the case for all measurements using the multithermal probe method.

III. RESULTS AND DISCUSSION

A. Overall features of the azimuthal motion in different aspect ratios

Figure 3 plots time traces of ϕ measured by the PIV technique in $\Gamma = 2.3$, 1, $1/2$ cells, respectively (all cells are leveled). In the figure, the time trace for $\Gamma = 1$ has been shown previously [24], for ease of comparison we replot it here. The figure shows that the azimuthal motion of the LSC in $\Gamma = 2.3$ cell is confined in much narrower azimuthal region than in the $\Gamma = 1$ and $\Gamma = 1/2$ cells. The striking feature of the trace for $\Gamma = 1$ is the existence of the plateau levels in ϕ, this "residence" phenomenon has been studied in detail previously [24]. In $\Gamma = 1/2$ cells, under the same leveling condition, ϕ is found to be much more erratic and the "residence"

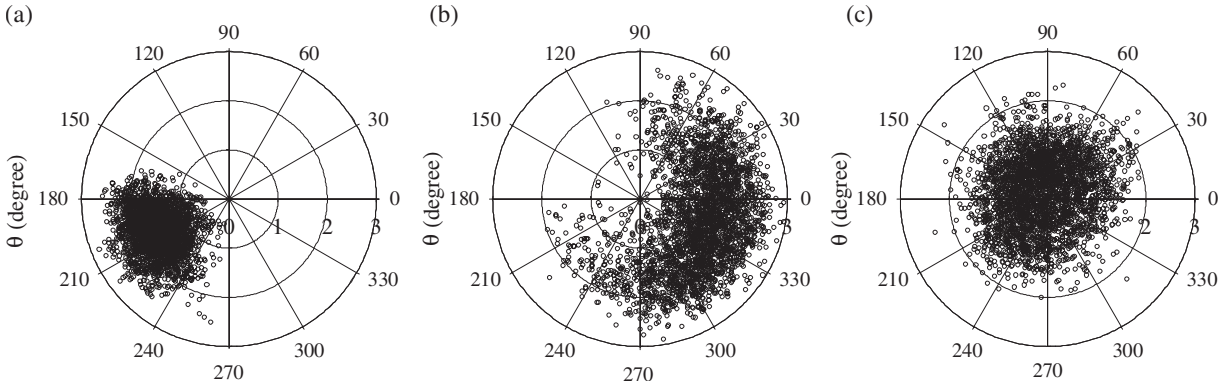

FIG. 4. The azimuthal orientation angle θ and flow magnitude V_{LSC} of the LSC plotted in polar coordinates. (a) $\Gamma=2.3$ ($\mathrm{Ra}=8.0\times10^{8}$), (b) $\Gamma=1$ ($\mathrm{Ra}=4.7\times10^{9}$), and (c) $\Gamma=1/2$ ($\mathrm{Ra}=5.3\times10^{10}$). The radial coordinate is the velocity in unit of cm/sec, the angular coordinate is the azimuthal angle in degrees. There are 3000 data points in each plot. All cells are leveled.

phenomenon is absent. To show clearly the range of the azimuthal angle that can be explored by the LSC, in Fig. 4 we plot $\vec{V}_{\mathrm{LSC}}$ in polar coordinates. In this plot both the amplitude V_{LSC} and the orientation θ of $\vec{V}_{\mathrm{LSC}}$ are displayed, and 3000 data points are plotted for each Γ, which corresponds to measurements spanning about 50–100 turnover times of the LSC. From the figure the differences are obvious; in the $\Gamma=2.3$ cell azimuthal motion of the LSC is highly confined in both angular range and the magnitude of the velocity (note that V_{LSC} never goes down to zero); in $\Gamma=1$ the LSC can explore more azimuthal region and the velocity magnitude also has much larger fluctuations; and in $\Gamma=1/2$ the LSC can reach any azimuthal orientation with nearly equal probability and cessations ($V_{\mathrm{LSC}}\simeq0$) occur much more frequently which is consistent with our previous finding [38]. The above results suggest that the LSC's azimuthal motion is more confined in larger Γ geometries.

Long time measurements of the LSC orientations θ_{bot}, θ_{mid}, and θ_{top} and strengths A_{bot}, A_{mid}, and A_{top} at the three heights by the multithermal-probe method are carried out for $\Gamma=1$ and $1/2$, respectively. For each Γ, measurements are performed for at least five Ra, with most of them lasting longer than 2 days. Since in these two geometries the orientations of the LSC obtained at the three heights are almost the same [25,38], except stated otherwise, we will only show the result from the middle row thermistors.

An interesting feature of the LSC is its preferred orientation. This appears to be against intuition, as the cylindrical geometry implies that the LSC would take any azimuthal orientation with equal probability. Figure 5(a) shows the probability density function (PDF) of the orientation θ_{mid} of the LSC for both $\Gamma=1$ and $\Gamma=1/2$, both cells are leveled to $0\pm0.057°$. It is striking that the orientation plane of the LSC has a very strong preferred orientation in $\Gamma=1$ geometry. It is also found that the preferred orientation exists for all values of Ra studied. The fact that the LSC has a preferred orientation in $\Gamma=1$ geometry has been reported previously [7,11,23,24]. In contrast to the prominent preferred orientation in the $\Gamma=1$ case, the LSC has a much weaker preferred orientation in the $\Gamma=1/2$ geometry, which implies that the LSC's vertical circulation plane can explore any azimuthal position with nearly equal probability. The difference between the two geometries may be quantified by the standard deviation $\sigma_{\theta_{\mathrm{mid}}}$ of θ_{mid}, which is plotted in Fig. 5(b) as a function of Ra for both values of Γ. It is seen that $\sigma_{\theta_{\mathrm{mid}}}$ in $\Gamma=1/2$ geometry is about twice as larger as that in the $\Gamma=1$ geometry, and there is no obvious Ra dependence for each Γ. Recently Brown and Ahlers (BA) proposed a model to explain the observed preferred orientation and net rotations of the LSC [37]. The model explicitly considers the effect of the Coriolis force and one of its assumptions is the existence of a single roll structure of the LSC, which holds in both the $\Gamma=1$ and $1/2$ geometries. In the model the LSC flow is divided into four parts: two segments of vertical flow and two segments of horizontal flow. Force analysis for the

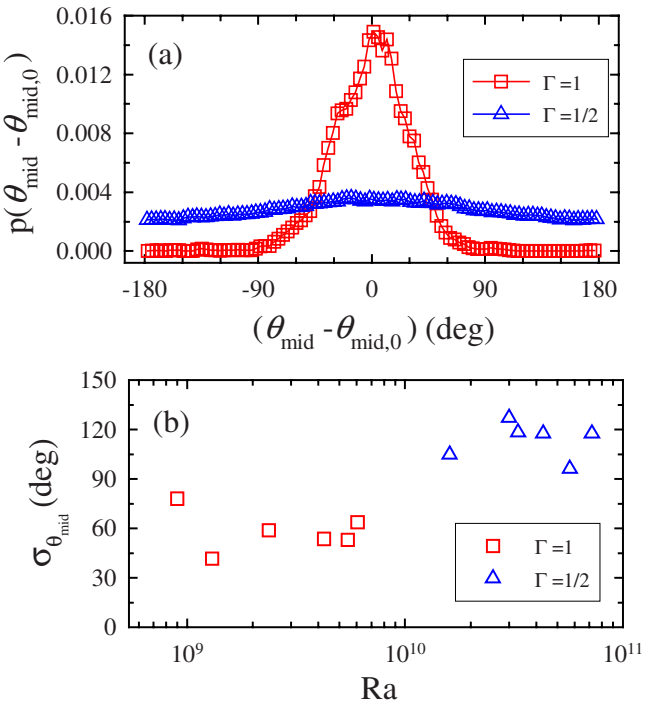

FIG. 5. (Color online) (a) The probability density function (PDF) of $\theta_{\mathrm{mid}}-\theta_{\mathrm{mid},0}$ for $\Gamma=1$ ($\mathrm{Ra}=2.4\times10^{9}$) and for $\Gamma=1/2$ ($\mathrm{Ra}=5.7\times10^{10}$) geometries, where $\theta_{\mathrm{mid},0}$ is the preferred orientation. (b) The standard deviation $\sigma_{\theta_{\mathrm{mid}}}$ of θ_{mid} as function of Ra for $\Gamma=1$ and $1/2$.

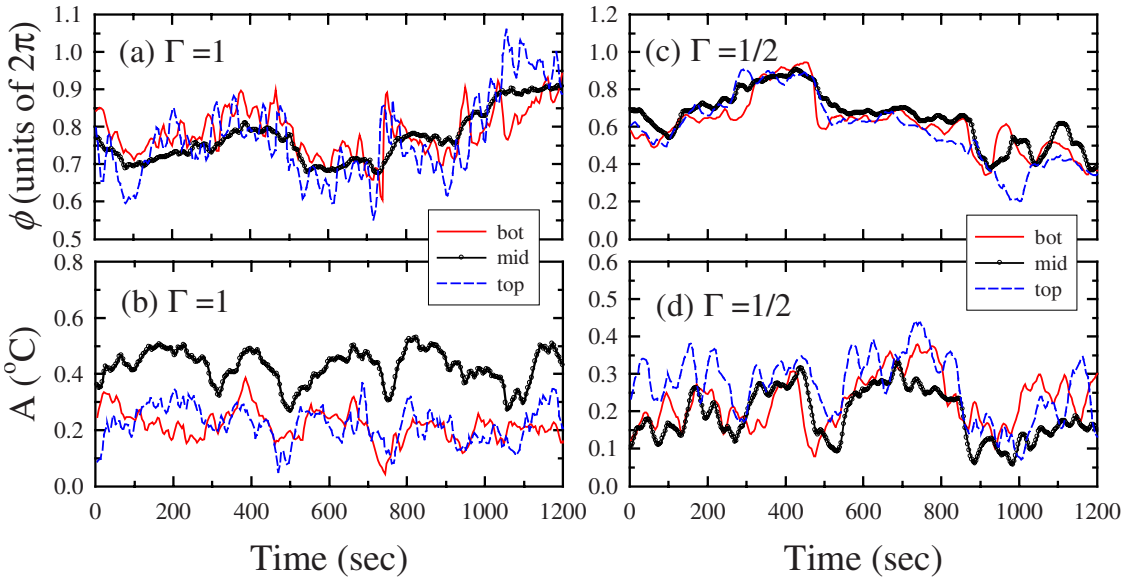

FIG. 6. (Color online) (a) and (c) Segments of time traces of the orientations ϕ; (b) and (d) the corresponding amplitudes A for $\Gamma=1$ ($\mathrm{Ra}=5.5\times10^9$) and $\Gamma=1/2$ ($\mathrm{Ra}=7.2\times10^{10}$), respectively.

individual segments shows that the vertical flow induces a preferred orientation (up flow to the west and down flow to the east) and the horizontal flow generates a net rotation in the clockwise direction. According to the model, in both $\Gamma=1$ and $1/2$ geometries the LSC would have a strong preferred orientation. However, our previous result in the $\Gamma=1$ geometry shows that although the preferred orientations exist [24], it is not unique as the model predicted. Further more the much flatter PDF of orientation θ in $\Gamma=1/2$ cell in the present study is not consistent with a strong preferred orientation. In addition, if the Coriolis plays a crucial role, in $\Gamma=1/2$ cells the torque induced by the Coriolis force will be larger than that in $\Gamma=1$ cells as the vertical flows occupy larger volume in $\Gamma=1/2$ cells, thus could lock the LSC within a narrower azimuthal range than that in $\Gamma=1$ cell, which is obvious not the case as shown in Fig. 5. The origin of the inconsistency between the BA model and our results regarding the preferred orientation is presently not known to us.

B. Oscillatory and diffusive motions of the azimuthal orientation

To examine the azimuthal motion in more detail, we show in Figs. 6(a) and 6(b) segments of time traces of the LSC orientations and amplitudes obtained at the three heights for $\Gamma=1$ and $1/2$. It is clear that for $\Gamma=1$ both ϕ_{bot} and ϕ_{top} oscillate over short time scales and fluctuate erratically in longer time scales. In addition, the oscillations of ϕ_{bot} and ϕ_{top} have a 180° phase difference, which is confirmed by the cross-correlation function between these two quantities (not shown here). The oscillations of ϕ_{bot} and ϕ_{top} are also evident from the prominent peak in their respective power spectrum, as shown in Fig. 7(a). It is clear from both the time trace and the power spectrum that the azimuthal oscillation is absent at the midheight. Please also note that the slopes of the power spectra of ϕ in the log-log plot are close to -2, suggesting a Brownian-type behavior of azimuthal motion of LSC. The diffusive behavior of the azimuthal motion was first observed in the $\Gamma=1/2$ geometry [12] and later also in $\Gamma=1$ cells [24].

The oscillation periods τ_0 of ϕ_{bot} and of ϕ_{top} are very close to each other (39.2 and 38.3 s at $\mathrm{Ra}=5.5\times10^9$). This is the same azimuthal oscillation that has been found in previous studies [24,25,42]. It is also interesting that the period of the azimuthal oscillation is essentially the same as those of the local temperature and velocity oscillations measured at midheight within the vertical circulation plane of the LSC [43,44]. How these two types of apparently different motions are connected has been a mystery. Please see Refs. [45,46] for the latest development on this problem. The flow strength A_{bot} and A_{top} measured near the bottom and top plates also show weak oscillations. This oscillation is not so obvious from the time trace [shown in Fig. 6(b)], but can be seen from the power spectra shown in Fig. 7(b). This suggests that the oscillation of the LSC's magnitude is much less coherent than that of its orientation. The much weaker oscillation of the LSC's magnitude compared to that of its orientation has in fact been observed in a previous study using direct velocity measurement [24]. The above results show that in $\Gamma=1$ geometry the top and bottom parts of the LSC constantly undergo a twisting motion over the time scale of the LSC's turnover time measured in a vertical plane, while over longer time scales the LSC as a whole moves erratically in a diffusive manner. These results are consistent with previous findings using both the shadowgraph and temperature measurements [24–26].

In Figs. 6(c) and 6(d) we show the time series of ϕ and A measured in the $\Gamma=1/2$ cell. It is seen that neither the orientation nor the amplitude of the LSC show any oscillatory behavior, which can also be seen from the respective power spectra shown in Figs. 7(c) and 7(d). Thus, the twisting motion of the LSC found in $\Gamma=1$ geometry is absent in the $1/2$ case. It should be noted that previous local temperature and

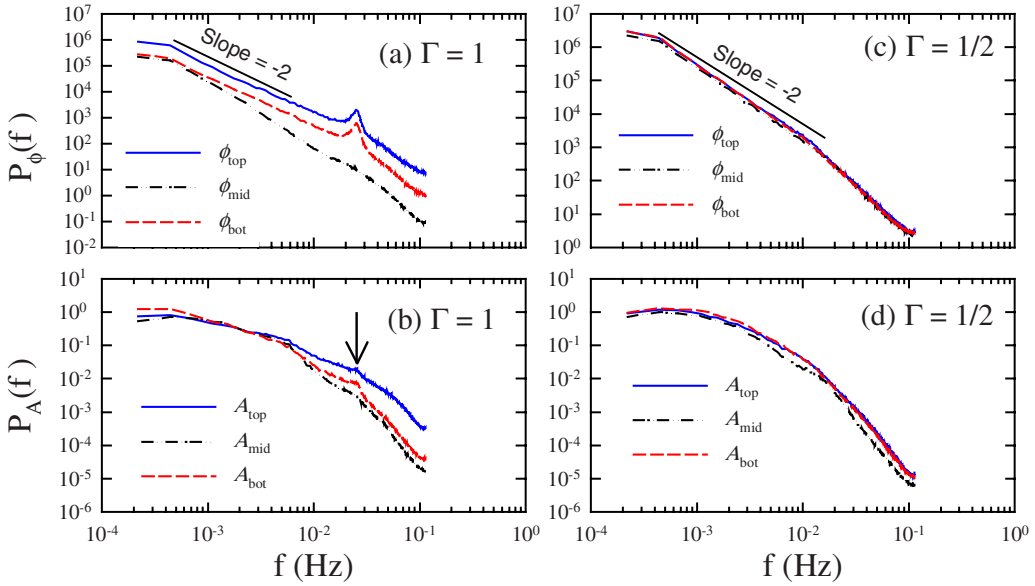

FIG. 7. (Color online) The power spectra of the orientations $P_\phi(f)$ and flow strengths $P_A(f)$ of LSC measured at the three heights. (a) and (b) $\Gamma=1$ ($\mathrm{Ra}=5.6\times10^9$); (c) and (d) $\Gamma=1/2$ ($\mathrm{Ra}=5.7\times10^{10}$).

velocity measurements made at midheight and within the vertical circulating plane of the LSC exhibit oscillations in the $\Gamma=1$ geometry but not in the $\Gamma=1/2$ case [5,8,10,13,44,47]. Thus, it appears that the azimuthal twisting oscillation near top and bottom plates and the local velocity and temperature oscillations at midheight near sidewall are concomitant features, i.e., if one type of oscillation is missing (present) in a particular geometry the other type will also be absent (present) in the same geometry. This suggests that there is a single mechanism driving both types of oscillations, or it is simply the same oscillation manifested in different ways. Similar to the $\Gamma=1$ case, the power spectra of the measured ϕ in the $\Gamma=1/2$ geometry all have slopes very close to -2 in log-log scale [Fig. 7(c)], which is consistent with the diffusive behavior found in a previous study [12] for this geometry.

C. Reorientations of the LSC

From above it is seen that the long time trend of the LSC's orientation is a diffusion-type motion. Each of the erratic move leads to a change of the LSC's azimuthal orientation from its previous position. Through closer examination it is seen that there are large number of such reorientation events contained in the time series of ϕ measured in both $\Gamma=1$ and $1/2$ geometries (Fig. 6). The reorientation of the LSC can be accomplished by either azimuthal rotations or cessations. A rotation-led reorientation is accomplished by a rotation of the LSC's vertical circulating plane without significant variation of its flow strength. An example of this type of reorientation is shown in Figs. 8(a) and 8(b). A cessation-led reorientation is a process during which the LSC momentarily loses its flow strength, then restarts at a new orientation. An example of reorientation as a result of cessation is shown in Figs. 8(c) and 8(d). From Fig. 8 it is obvious that for a comparable value of the azimuthal angular change reorientations arising from cessations occur over much shorter time scales than those arising from rotations. It has been found that after a cessation, the LSC can start in any orientation, including the original one, and when the orientational change is 180° it results in a flow reversal. Note that reversals defined this way is just a subset of cessations and is different from those resulting from a 180° azimuthal rotation of the LSC circulation plane. Previous studies have found that in $\Gamma=1$ geometry, the angular change after a cessation has a uniform distribution over all possible values [23,25], and so reversals are rare events among cessations. Whereas, it was found in the $\Gamma=1/2$ geometry that reversals are the most probable events after a cessation [38]. Hence, the dynamics of cessations and reversals in the two geometries appear to be governed by different mechanisms. As cessations (and reversals) are a subset of reorientations, it would be therefore interesting to know whether the more general events of reorientations are in anyway different in the two geometries. Here we present a comparative analysis of the

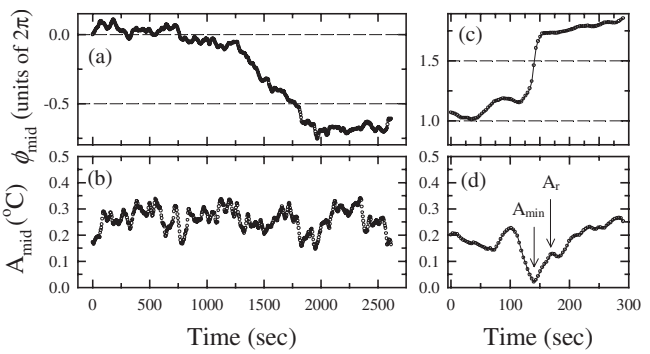

FIG. 8. (a) and (b): an example of rotation-led reorientation. (c) and (d): an example of cessation-led reorientation events ($\Gamma=1/2$, $\mathrm{Ra}=5.7\times10^{10}$). $A_{\min}$ is the minimum value of A reached in the cessation or reversal and A_r is the local maximum of A after it rebounds from $A_{\min}$.

reorientation events in the two geometries regardless whether the reorientation is generated as a result of rotation or cessation.

Operationally we define a reorientation as an azimuthal angular change satisfying two conditions. First, the net orientational change over a set of successive data points for ϕ should be larger than $|\Delta\phi|_{\min}$, and second the average net rotation rate over that period should be larger than $\dot{\phi}_{\min}$. These two criteria are similar to those used by Brown and Ahlers [23,25]. For the $\Gamma=1$ cell, we explored the parameter range: $1^\circ < \dot{\phi}_{\min}\tau_0 < 4^\circ$ and $10^\circ < |\Delta\phi|_{\min} < 45^\circ$, and found that the events obtained with different thresholds in these parameter ranges produce similar statistics. So we adopted $\dot{\phi}_{\min}\tau_0 = 2^\circ$ and $|\Delta\phi|_{\min} = 20^\circ$ as the criteria for identifying reorientation events. From the 31-day measurement in $\Gamma=1$ cell with $\mathrm{Ra}=5.6\times10^9$, 3136 reorientation events are identified. For the cell with $\Gamma=1/2$, we explored the parameter range $0.5^\circ < \dot{\phi}_{\min}\tau_0 < 6^\circ$ and $6^\circ < |\Delta\phi|_{\min} < 90^\circ$, and found that the events obtained with different thresholds in these parameter ranges again give similar statistics. We therefore used $\dot{\phi}_{\min}\tau_0 = 3^\circ$ and $|\Delta\phi|_{\min} = 45^\circ$ as the criteria for identifying reorientation events for this geometry. For $\Gamma=1/2$, from 34-day measurement with $\mathrm{Ra}=5.7\times10^{10}$, 7072 reorientation events are obtained. We emphasize that the different values of threshold used above will change only the number of identified reorientation events but they will not influence the statistical properties of reorientations for the two geometries to be presented below.

We study first the time interval τ_1 between neighboring reorientations. The PDF of τ_1 for $\Gamma=1$ and $1/2$, normalized by their respective averages, are shown in Figs. 9(a) and 9(b), respectively. In both cases, the data can be fitted excellently to $p(\tau_1/\langle\tau_1\rangle)=\exp(-\tau_1/\langle\tau_1\rangle)$, suggesting that the occurrence of the reorientations is a Poisson process, i.e., the reorientation has no memory and the neighboring events are independent of each other. The exponentially distributed τ_1 in $\Gamma=1$ is consistent with previous findings [23,25], and here we find that this property holds also in $\Gamma=1/2$ geometry. Shown in the insets of Figs. 9(a) and 9(b) are the Ra dependence of the reorientation frequency f_r for the two geometries, respectively, here $f_r=1/\langle\tau_1\rangle$. For $\Gamma=1$, f_r is seen to have increased by roughly a factor of 2 over a decade of Ra, which is consistent with a previous result [25]. For $\Gamma=1/2$, f_r is larger than that in $\Gamma=1$ cells, but appears to have a much weaker Ra dependence.

We examine next the orientational change $|\Delta\phi|$ of the LSC through a reorientation. Figure 10(a) shows the PDF of $|\Delta\phi|$ for $\Gamma=1$ in a log-log plot, and Fig. 10(b) shows the PDF of $|\Delta\phi|$ for $\Gamma=1/2$ in a semilog plot. The straight line in Fig. 10(a) is a power-law fitting, which clearly fits the data very well. The slope of the power law fit is -3.3, which is within exponent range of -3.25 to -4.45 obtained for different values of Ra by Brown and Ahlers [23,25].

In $\Gamma=1/2$ geometry, however, the situation is clearly different. As shown in Fig. 10(b), $|\Delta\phi|$ is distributed exponentially. The inset plots the same data in log-log scale, with the same solid line as in the main figure, i.e., an exponential fit. Again, it shows clearly that the data follows an exponential distribution rather than a power-law one. From Figs. 10(a) and 10(b), we can also see that in $\Gamma=1/2$ cells reorientations with large orientational change is more probable than those in $\Gamma=1$ cells. As cessations is a subset of reorientations, the above result is consistent with a recent finding that in the $\Gamma=1/2$ geometry the most probable cessation events are reversals [38]. Figures 10(c) and 10(d) show, respectively, for $\Gamma=1$ and $1/2$, the PDFs of the orientation of LSC at the start, and at the end, of a reorientation, ϕ_{initial} and ϕ_{final}. Also shown in the figure is the PDF of ϕ itself. Please note that here ϕ_{initial} and ϕ_{final} are reduced to within $[0, 360^\circ]$, ϕ is also reduced within $[0, 360^\circ]$ (so that it now represents the physical orientation of LSC). The PDFs of ϕ_{initial} and ϕ_{final} are very close to that of ϕ, implying that the reorientation can start, and end, at any orientation.

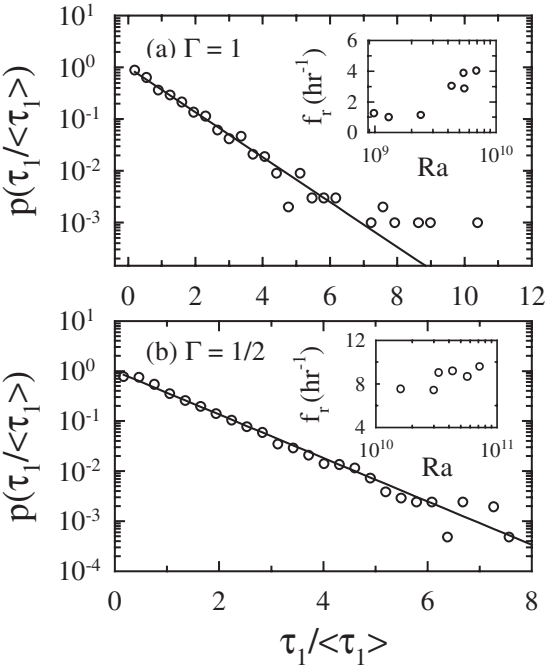

FIG. 9. (a) The PDF of the time interval τ_1 of the neighboring reorientations for $\Gamma=1$ ($\mathrm{Ra}=5.6\times10^9$). (b) PDF of τ_1 for $\Gamma=1/2$ ($\mathrm{Ra}=5.7\times10^{10}$). The insets in both figures are the frequency of reorientation f_r as functions of Ra for the respective aspect ratios.

The above results, together with those from an earlier study [38], demonstrate clearly that the dynamics of reorientations, in the aspect ratio 1 and $1/2$ geometries appear to be governed by different mechanisms, whether this is with respect to the general reorientation events or a subset (i.e., cessations or reversals) of it. A recent theoretical model appears to have explained well the observed properties of reorientations, cessations, and reversals for $\Gamma=1$ case [32]. Further study in future is of course needed to incorporate also the result for $\Gamma=1/2$ case.

D. Cessations and reversals of the LSC

In Fig. 8(b), we have shown an example of cessation. In this example the cessation is accompanied by an orientation change of approximately 180°, which is thus a flow reversal. It is seen from the figure that the timescale in which the orientational change itself takes place is much shorter than

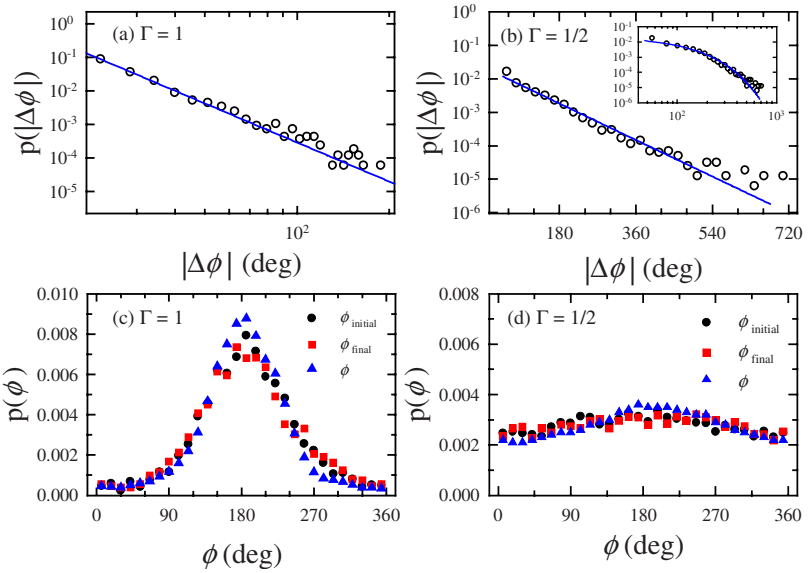

FIG. 10. (Color online) (a) PDF of the orientation change $|\Delta\phi|$ through reorientation for $\Gamma=1$. The straight line represents a power-law fit to the data. (b) PDF of $|\Delta\phi|$ for $\Gamma=1/2$. The straight line represents an exponential fit to the data. Inset: the same data in log-log scale. (c) The PDF of the LSC orientation ϕ_{initial} at the start, and that of ϕ_{final} at the end, of reorientations for $\Gamma=1$, also shown is the PDF of the LSC orientation ϕ itself. (d) The PDF of ϕ_{initial} and ϕ_{final} for $\Gamma=1/2$, also shown is the PDF of the LSC orientation ϕ itself.

that it takes the flow strength to decline before, and then rebound after, the orientational change. We find that, on average, the "reversal process" (or change of ϕ) does not start until the flow strength has declined about 90% of the previous maximum. This is qualitatively similar to those found from records of geomagnetic reversals [48–50]. As has been shown previously that in $\Gamma=1$ cells cessations occur randomly with very low frequency (about 1.5/day) [23,25]. On the other hand, we have recently found that in $\Gamma=1/2$ cells both cessations and reversals occur much more frequently [38]. Thus a statistically significant number of cessations and unambiguously identified reversal events have been obtained in this geometry. The reversal of the flow direction of the LSC in the RB system resembles many reversal phenomena occurring in nature. An interesting question to ask is therefore: Can one predict when the next cessation or reversal will occur? We have shown in Ref. [38] that the time interval t_1 between successive reversals are exponentially distributed, which means that the occurrence of reversals is independent to each other. In this sense, as far as the time interval between events is concerned, the cessation or reversal is a Poisson process, thus one cannot predict when the next cessation or reversal will occur. However, if more information is included, such as those about the flow strength change during a cessation or reversal, the cessation or reversal may not be unpredictable.

Paleomagnetic records revealed that a larger rebound of the geomagnetic field intensity after a reversal usually results in a longer period of time without reversals [48]. It is natural to ask if the situation is similar for the flow direction reversal of the LSC in the RB system. To this end we analyze the statistical properties of flow intensity change and related time scales during cessations and reversals. Denote $A_{\min}$ as the minimum value of A reached in the cessation or reversal and A_r as the local maximum of A after it rebounds from $A_{\min}$ [see Fig. 8(b)], the normalized "rebound amplitude" is then defined as $\delta A_r=(A_r-A_{\min})/\langle A\rangle$, where $\langle A\rangle$ is the average of A for the entire time series. Previously we have found that δA_r and the immediately following t_1 are positively correlated [38]. A stronger δA_r will lead a longer time period with no cessation or reversal. But we do not know in which way these two quantities are correlated. The relationship between the amplitude of rebound δA_r and the immediately following t_1 between cessations or reversals can be represented by the average value of t_1 for a particular value of δA_r, i.e., the conditional average $\langle t_1|\delta A_r\rangle$. Figures 11(a) and 11(b) plot $\langle t_1|\delta A_r\rangle/\tau_0$ vs δA_r for cessations and reversals, respectively. They show that a larger rebound of the flow strength of the LSC leads to a longer period of time without cessations or reversals, which can also be seen from the strong positive correlation between δA_r and t_1 [38]. To further study the relationship between the rebound strength and the time interval t_1 between cessations or reversals, we fit the data with an exponential rise function $\langle t_1|\delta A_r\rangle/\tau_0=a(1-e^{-\delta A_r/b})$ as shown in Fig. 11. The fitted parameters are $a=15.7$, $b=0.42$ for cessation and $a=183.7$, $b=0.20$ for reversal, respectively. There is an upper bound of the function, the statistical aver-

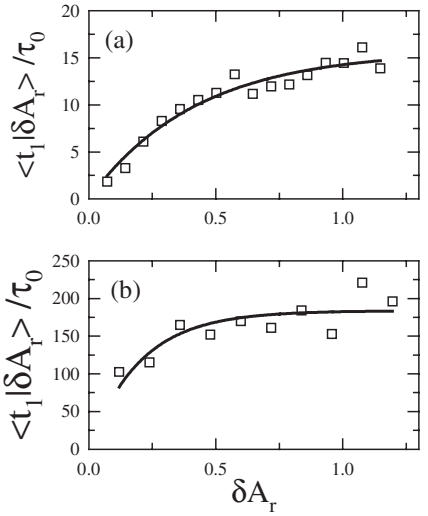

FIG. 11. The normalized conditional average $\langle t_1|\delta A_r\rangle/\tau_0$ of t_1 on the rebound amplitude δA_r for (a) cessations and (b) reversals. The solid lines are fittings of the exponential rise function $\langle t_1|\delta A_r\rangle/\tau_0=a(1-e^{-\delta A_r/b})$ to the data. The data are measured in the $\Gamma=1/2$ cell at $\text{Ra}=5.7\times10^{10}$.

aged maximum time interval between cessations or reversals—a, which suggests that the time interval between the cessation or reversal cannot be extremely large. The scale of characteristic flow strength for the exponential rise function $\langle t_1 | \delta A_r \rangle / \tau_0 = a(1-e^{-\delta A_r/b})$ are $b\langle A \rangle = 0.42\langle A \rangle$ and $b\langle A \rangle = 0.20\langle A \rangle$ for cessations and reversals, respectively. The figure shows that, for a given rebound flow strength, we can indeed predict when it is most likely to occur.

It is interesting to note that palaeomagnetic records also show similar correlation between the strength of field intensity rebound and the time interval between adjacent polarity reversals of geomagnetic field [48]. Although it is generally believed that the reversal of the geomagnetic field is caused by the reversal of the convective flow in the outer core of the Earth, it is obvious that the flow in the idealized RB convection is different in many ways from the convective flow of the Earth's outer core, which is additionally influenced by magnetic and Coriolis forces. Thus our result cannot be directly used to predict the next reversal of the geomagnetic field. But if the reversal phenomenon occurring in a wide variety of fluid flows share some universal features and the idealized RB system is able to capture some of the essential features of the phenomenon, the study of the statistical properties of the reversals in the RB system may shed some light to the more complicated reversals of geomagnetic field.

IV. CONCLUSION

In this paper we have reported measurements of the orientation and the flow strength of the large-scale circulation (LSC) in Rayleigh-Bénard convection. For aspect ratios $\Gamma = 2.3$, 1, and $1/2$ direct velocity measurement reveals that with increasing aspect ratio the azimuthal motion of the LSC is increasingly confined in smaller angular regions. A detailed comparative study of the azimuthal motion between the aspect ratios $\Gamma = 1$ and $1/2$ geometries are then made using long time measurements (over 30 days each) based on indirect multithermal-probe measurement.

It is found that the twisting azimuthal oscillation of the LSC observed in $\Gamma = 1$ geometry is absent in the $\Gamma = 1/2$ geometry. For both $\Gamma = 1$ and $1/2$, the overall trend of the erratic azimuthal motions of the LSC is found to be diffusive in nature. The dynamics of reorientations, however, are found to exhibit different properties in the two geometries. For $\Gamma = 1/2$, the orientational change $|\Delta\phi|$ is found be distributed exponentially, and that larger $|\Delta\phi|$ are more probable than those in $\Gamma = 1$ case. For $\Gamma = 1$, $|\Delta\phi|$ through a reorientation is found to be power-law distributed, which is consistent with previous findings. Despite the difference in orientational change, the occurrence of the reorientations is found to be a Poisson process for both geometries. Using the large number of unambiguously identified cessation or reversal events in $\Gamma = 1/2$ geometry, we have shown that the average value of the time interval between neighboring cessations or reversals conditioned on the rebound flow strength follows an exponential rise function, thus demonstrating the possibility to empirically forecast the time the next cessation or reversal will most likely occur if the rebound flow strength of the preceding cessation or reversal is given.

ACKNOWLEDGMENTS

We thank Quan Zhou for his help in the direct velocity measurement of the LSC. This work was supported by the Research Grants Council of Hong Kong SAR under Grant No. 403806.

APPENDIX: LEVELLING THE CONVECTION CELL

The flow and the heat transport are very sensitive to the levelling condition of the convection cell. To make the cell as leveled as possible, we made an apparatus to measure its leveling condition. The apparatus is similar to a pendulum, a plumb is hung over a post by a wire, the post itself is fixed on a stand. If the cell is tilted with a small angle γ, when the apparatus is put on the top plate of the cell (we assume the top surface of the top plate is a smooth plane), the plumb tip will point to a point, denoted by P_1, at the stand. Then we rotate the stand along the vertical axis by 180°, the plumb tip will point to another position P_2 at the stand, due to the tilt of the cell. Thus the middle point P_3 between P_1 and P_2 is obtained, since γ is very small, it can be calculated by $\gamma = d_{P_1P_3}/L$, where $d_{P_1P_3}$ is the distance between P_1 and P_2, L is the length of the wire which is 1 m here. When the plate is adjusted to let the plumb points to P_3, the cell is leveled. The accuracy in determining the position of P_3 is 1 mm, thus the accuracy of the level condition is 1 mm/1000 mm (rad) = 0.057°. In the experiment, we first make sure that the two plates are parallel, thus when the top plate is leveled, the cell is leveled.

[1] L. P. Kadanoff, Phys. Today **54**, 34 (2001).
[2] A. Davaille and J. Vatteville, Geophys. Res. Lett. **32**, L14309 (2005).
[3] R. Krishnamurti and L. N. Howard, Proc. Natl. Acad. Sci. U.S.A. **78**, 1981 (1981).
[4] M. Sano, X.-Z. Wu, and A. Libchaber, Phys. Rev. A **40**, 6421 (1989).
[5] B. Castaing, G. Gunaratne, F. Heslot, L. Kadanoff, A. Libchaber, S. Thomae, X.-Z. Wu, S. Zaleski, and G. Zanetti, J. Fluid Mech. **204**, 1 (1989).
[6] S. Ciliberto, S. Cioni, and C. Laroche, Phys. Rev. E **54**, R5901 (1996).
[7] S. Cioni, S. Ciliberto, and J. Sommeria, J. Fluid Mech. **335**, 111 (1997).
[8] X.-L. Qiu and P. Tong, Phys. Rev. E **64**, 036304 (2001).
[9] K.-Q. Xia, C. Sun, and S.-Q. Zhou, Phys. Rev. E **68**, 066303 (2003).
[10] X.-L. Qiu, X.-D. Shang, P. Tong, and K.-Q. Xia, Phys. Fluids **16**, 412 (2004).
[11] C. Sun, K.-Q. Xia, and P. Tong, Phys. Rev. E **72**, 026302

(2005).
[12] C. Sun, H.-D. Xi, and K.-Q. Xia, Phys. Rev. Lett. **95**, 074502 (2005).
[13] Y. Tsuji, T. Mizuno, T. Mashiko, and M. Sano, Phys. Rev. Lett. **94**, 034501 (2005).
[14] T. Haramina and A. Tilgner, Phys. Rev. E **69**, 056306 (2004).
[15] E. Calzavarini, D. Lohse, F. Toschi, and R. Tripiccione, Phys. Fluids **17**, 055107 (2005).
[16] G. Stringano and R. Verzicco, J. Fluid Mech. **548**, 1 (2006).
[17] S. Kenjereš and K. Hanjalić, Phys. Rev. E **66**, 036307 (2002).
[18] R. Verzicco and R. Camussi, J. Fluid Mech. **477**, 19 (2003).
[19] E. Villermaux, Phys. Rev. Lett. **75**, 4618 (1995).
[20] H.-D. Xi, S. Lam, and K.-Q. Xia, J. Fluid Mech. **503**, 47 (2004).
[21] H.-D. Xi and K.-Q. Xia, Phys. Fluids **20**, 055104 (2008).
[22] S. Cioni, S. Ciliberto, and J. Sommeria, Dyn. Atmos. Oceans **24**, 117 (1996).
[23] E. Brown, A. Nikolaenko, and G. Ahlers, Phys. Rev. Lett. **95**, 084503 (2005).
[24] H.-D. Xi, Q. Zhou, and K.-Q. Xia, Phys. Rev. E **73**, 056312 (2006).
[25] E. Brown and G. Ahlers, J. Fluid Mech. **568**, 351 (2006).
[26] D. Funfschilling and G. Ahlers, Phys. Rev. Lett. **92**, 194502 (2004); D. Funfschilling, E. Brown, and G. Ahlers, J. Fluid Mech. **607**, 119 (2008).
[27] U. Hansen, D. A. Yuen, and S. E. Kroening, Geophys. Astrophys. Fluid Dyn. **63**, 67 (1992).
[28] K. R. Sreenivasan, A. Bershadskii, and J. J. Niemela, Phys. Rev. E **65**, 056306 (2002).
[29] R. Benzi, Phys. Rev. Lett. **95**, 024502 (2005).
[30] R. Benzi and R. Verzicco, Europhys. Lett. **81**, 64008 (2008).
[31] F. F. Araujo, S. Grossmann, and D. Lohse, Phys. Rev. Lett. **95**, 084502 (2005).
[32] E. Brown and G. Ahlers, Phys. Rev. Lett. **98**, 134501 (2007); E. Brown and G. Ahlers, Phys. Fluids **20**, 075101 (2008).
[33] J. J. Niemela, L. Skrbek, K. R. Sreenivasan, and R. J. Donnelly, J. Fluid Mech. **449**, 169 (2001).
[34] J. Sommeria, J. Fluid Mech. **170**, 139 (1986).
[35] G. A. Glatzmaier, R. S. Coe, L. Hongre, and P. H. Roberts, Nature (London) **401**, 885 (1999).
[36] E. van Doorn, B. Dhruva, K. Sreenivasan, and V. Cassella, Phys. Fluids **12**, 1529 (2000).
[37] E. Brown and G. Ahlers, Phys. Fluids **18**, 125108 (2006).
[38] H.-D. Xi and K.-Q. Xia, Phys. Rev. E **75**, 066307 (2007).
[39] S.-L. Lui and K.-Q. Xia, Phys. Rev. E **57**, 5494 (1998).
[40] C. Sun and K.-Q. Xia, J. Fluid Mech. **570**, 479 (2007).
[41] G. Ahlers, E. Brown, and A. Nikolaenko, J. Fluid Mech. **557**, 347 (2006).
[42] C. Resagk, R. du Puits, A. Thess, F. V. Dolzhansky, S. Grossmann, F. F. Araujo, and D. Lohse, Phys. Fluids **18**, 095105 (2006).
[43] X.-L. Qiu and P. Tong, Phys. Rev. E **66**, 026308 (2002).
[44] X.-D. Shang and K.-Q. Xia, Phys. Rev. E **64**, 065301(R) (2001).
[45] H.-D. Xi, S.-Q. Zhou, Q. Zhou, T.-S. Chan, and K.-Q. Xia, e-print arXiv:0806.4882v1.
[46] Q. Zhou, H.-D. Xi, S.-Q. Zhou, and K.-Q. Xia, e-print arXiv:0808.1171v1.
[47] X.-Z. Wu and A. Libchaber, Phys. Rev. A **45**, 842 (1992).
[48] J. P. Valet and L. Meynadier, Nature (London) **366**, 234 (1993).
[49] J. A. Jacobs, *Reversals of the Earth's Magnetic Field* (Cambridge University Press, New York, 1994).
[50] J. A. Jacobs, Surv. Geophys. **19**, 139 (1998).